Available online at www.sciencedirect.com
ScienceDirect
Earth and Planetary Science Letters 261 (2007) 321–334
EPSL
www.elsevier.com/locate/epsl

Basalt weathering across scales

Alexis Navarre-Sitchler [a,*], Susan Brantley [b]

[a] Department of Geosciences, The Pennsylvania State University, University Park PA 16802, United States
[b] Center for Environmental Kinetics Analysis, The Pennsylvania State University, University Park PA 16802, United States

Received 9 March 2007; received in revised form 2 July 2007; accepted 3 July 2007
Available online 17 July 2007
Editor: M.L. Delaney

Abstract

Weathering of silicate minerals impacts many geological and ecological processes. For example, the weathering of basalt contributes significantly to consumption of atmospheric carbon dioxide (CO_2) and must be included in global calculations of such consumption over geological timeframes. Here we compare weathering advance rates for basalt (w_D^β), where D and β indicate the scale at which the rate is determined and surface area measured, respectively, from the laboratory to the watershed scales. Data collected at the laboratory, weathering rind, soil profile and watershed scales show that weathering advance rate of basalt is a fractal property that can be described by a fractal dimension ($d_r \approx 2.3$). By combining the fractal description of rates with an Arrhenius relationship for basalt weathering, we derive the following equation to predict weathering advance rates at any spatial scale from weathering advance rates measured at the BET scale:

$$w_D^\beta = k_0 \left(\frac{\beta}{a}\right)^{d_r-2} e^{-E_a/RT}.$$

Here, k_0 is the pre-exponential factor (1.29×10^7 mm^3 mm^{-2} yr^{-1}), E_a is the activation energy (70 kj mol^{-1}), and a is a spatial constant related to the scale of measurement of BET surface area (10^{-7} mm). The term, $\left(\frac{\beta}{a}\right)^{d_r-2}$, is the roughness. The roughness fractal dimension can be conceptualized as a factor related to both the thickness of the reaction front and the specific surface area within the reaction front. However, the above equation can also be written in terms of a surface fractal dimension and the hypothetical average grain radius. These fractal dimensions provide insight into reaction front geometry and should vary with lithology. Once the surface area discrepancy has been accounted for using this method, we find a one to two order of magnitude range in weathering advance rates measured at any scale or temperature that can be attributed to factors such as changes in erosional regime, parent lithology, mechanism, climate, composition of reacting fluid, and biological activity. Our scaled equation, when used to predict global basalt CO_2 consumption based upon global lithologic maps, yields an uptake flux (1.75×1013 mol CO_2 yr^{-1}) within the predicted error of fluxes estimated based upon riverine measurements.

Keywords: basalt; weathering; fractal dimension; fractals; surface area; cation denudation rates; weathering advance rates; scaling

* Corresponding author.
E-mail address: anavarre@geosc.psu.edu (A. Navarre-Sitchler).

0012-821X/$ - see front matter © 2007 Elsevier B.V. All rights reserved.
doi:10.1016/j.epsl.2007.07.010

1. Introduction

At regional scales, weathering of minerals releases dissolved ions as nutrients available to vegetation (e.g. Hedin et al., 2003) or neutralizes catchments affected by acid rain (e.g. Johnson et al., 1981). At global scales, weathering influences the chemistry of the oceans and the regulation of atmospheric CO_2 concentrations over geologic time scales (e.g. Walker et al., 1981; Berner et al., 1983). To understand the mechanisms by which minerals dissolve, dissolution rates have been extensively studied in laboratory settings (White and Brantley, 1995). However, the comparison of these laboratory-derived rates to field scale studies is difficult due to the consistent trend that laboratory-derived rates are 2–5 orders of magnitude faster than field-derived rates for most phases (White and Brantley, 2003).

In general, extrapolation of weathering rates has relied upon using the mineral–water interfacial area as a scaling factor. For simplicity, we refer to this interfacial area here as the surface area. For example, many laboratory dissolution rates are normalized to the BET surface area (measured by sorption of gas molecules onto mineral powder) which assumes that all grains in the reactor are dissolving. However, watershed rates are normalized to geographic surface area because it is impossible to measure the BET surface area of all reacting grains in a watershed. Not surprisingly, the discussion and comparison of weathering rates have often separated mineral surface area-normalized rates and geographic surface area-normalized rates (e.g. Drever and Clow, 1995) and no consistent method has been derived that allows for an accurate comparison of laboratory- and field-derived rates.

Factors including erosion (Stallard, 1992; Riebe et al., 2004; West et al., 2005), composition of reacting fluid (e.g. Burch et al., 1993; Oelkers et al., 1994), and biological activity (e.g. Drever, 1994; Drever and Stillings, 1997; Lucas, 2001) vary from the laboratory to the field. Changes in these factors can contribute to differences in rates from laboratory to field. However, in at least some cases, the consistency of relative rates between laboratory and field studies indicates that a physical (surface area or hydrologic), rather than chemical or mechanistic difference is responsible for much of the difference in rates between scales (Velbel, 1993). Due to the difficulty of measuring surface area using the same methods at all scales, surface area estimations have been hypothesized to be a large contributor to what has been termed the "laboratory-field discrepency" (e.g. Schnoor, 1990; White and Peterson, 1990; Swoboda-Colberg and Drever, 1993; White, 1995; Brantley and Mellott, 2000; Brantley, 2003).

Surface area measurements on basalt indicate that surface area is a fractal property (e.g. Papelis et al., 2003). We use the fractal nature of surface area measurement to develop a method to integrate rates across spatial scales. To our knowledge this is the first systematic study of rates across scales for any lithology. We have chosen basalt because of its importance to the drawdown of atmospheric CO_2 from silicate weathering over geologic timescales. Based on watershed studies, an estimated 11.7×10^{12} mol of CO_2 are consumed annually by silicate weathering (Gaillardet et al., 1999) and 30–35% of that amount (4.08×10^{12} mol/yr) is attributed to basalt weathering (Dessert et al., 2003). The integration across scales derived in this study will provide a framework for future studies to compare weathering rates measured in the field with rates predicted from models based on laboratory dissolution. In addition, the present work elucidates important variables in weathering systems that must be further investigated.

2. Weathering advance rates

We examine published basalt weathering rates at four spatial scales: denudation rates from basalt watersheds, rates of soil formation from soil profiles developed on basalt of known ages, rates of weathering rind formation on basalt clasts weathered for known durations, and rates of dissolution of basalt in the laboratory. At each of these scales, basalt weathers to produce solutes and regolith and either of these production rates can be used to estimate the rate. At the laboratory scale, regolith consists of precipitates adhering to parent grains or suspended in the reactor as well as any leached layers that have formed on reacting grains. At the weathering rind, soil profile, and watershed scales, regolith is the layer of weathered material lying above unaltered bedrock (Fig. 1).

At these field scales, analysis of composition vs. depth shows partial to complete depletion of cations at the top grading down to parent composition at depth (White, 2002). The interval over which the concentration of cations increases downward from regolith concentrations to original parent defines the thickness of the reaction front (h), the depth scale over which basalt is altering. The rate at which this reaction front moves downward into the bedrock is the weathering advance rate (w). Above the reaction front, where parent minerals are no longer present at parent concentrations, pore waters are under-saturated with respect to the parent minerals. At the bottom of the front, porewaters

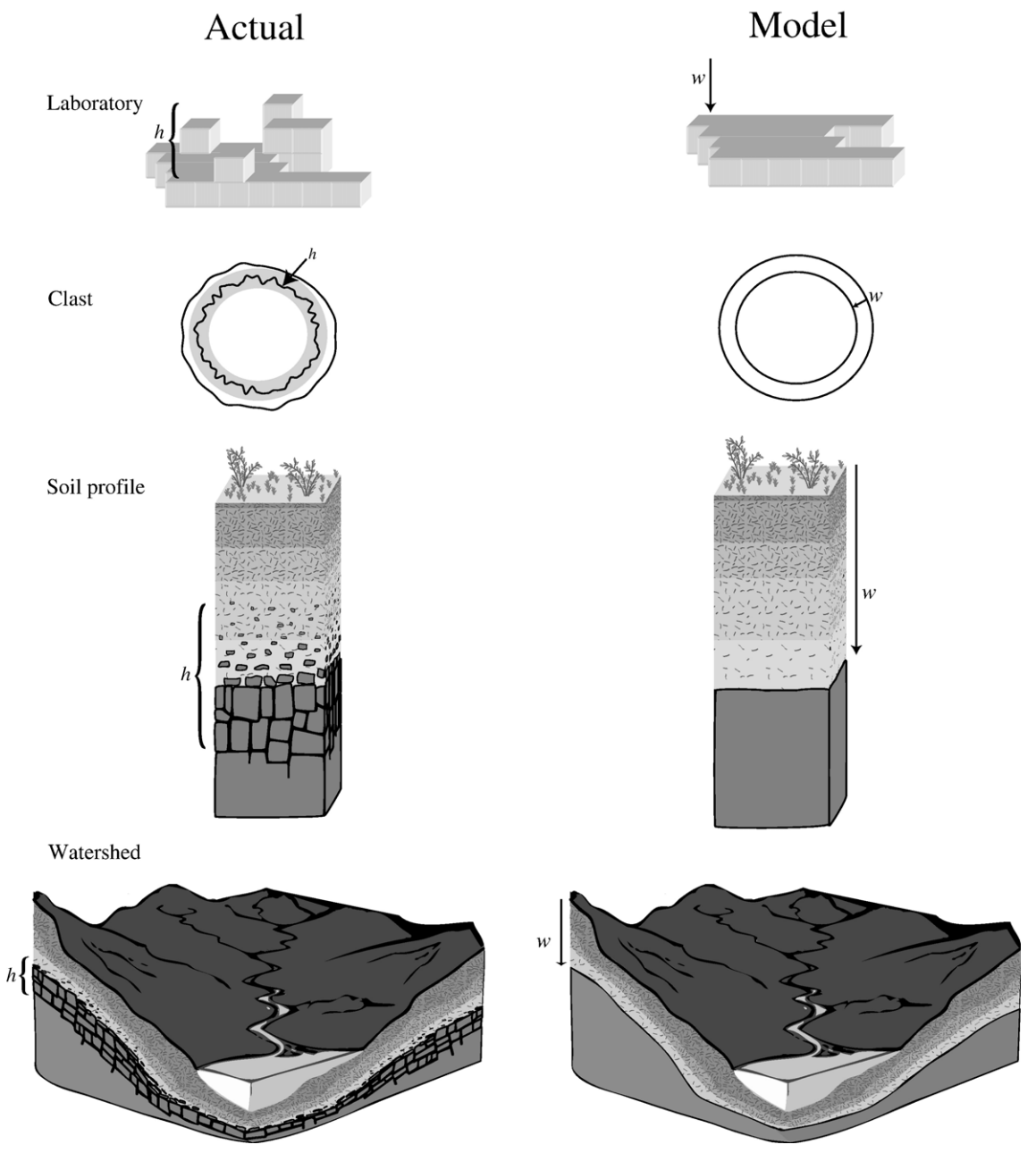

Fig. 1. Schematic diagrams of mineral, clast and soil profile scales observed (left) and conceptualized for modeling (right). The parameter h represents the thickness of the reaction front. This reaction front moves downward into the bedrock at the weathering advance rate, w (mm yr^{-1}). At each scale, the surface area is measured at a different resolution (β, not shown).

reach equilibrium with parent materials and dissolution is minimal. As minerals weather across the reaction front, therefore, at least two major processes occur: the interfacial mineral–water area changes and the saturation state of the pore fluid with respect to the parent minerals increases with depth. The thickness of the reaction front at each scale is determined by such properties as permeability, diffusivity, mineral reactivity, mechanical properties of the rock, biotic effects and grain size.

We define the weathering advance rate at a given scale D (w_D^{β}, mm^3 mm^{-2} yr^{-1}) as the volume of parent material transformed to (partially weathered) regolith

per unit time (Φ_{basalt}, mm^3 yr^{-1}) normalized by the total contributing surface area (s_D^β, mm^2):

$$w_D^\beta = \frac{\Phi_{basalt}}{s_D^\beta} \quad (1)$$

where D and β are related to the scales at which Φ_{basalt} and s are measured respectively. Specifically, the surface area term in Eq. (1) can be measured using different "rulers". At the laboratory scale (D=lab), surface area is either estimated using BET gas-adsorption (Brunauer et al., 1938; Brantley and Mellott, 2000) or using a geometric calculation from grain radius assuming spherical grains (e.g. Hodson, 2006). At higher scales, the surface area is estimated by the Euclidean surface area of the clast (D=rind), soil (D=soil), or watershed surface (D=ws). We define β to be the resolution of this surface area estimate at each scale: β=a, b, c, d, e for BET, geometric, clast, soil, and watershed respectively. For example, for a laboratory rate measurement normalized by a BET surface area, surface area is measured using gas molecules with radius on the order of 10^{-7} mm; therefore $a=10^{-7}$ mm. In contrast, when geometric surface area is calculated from grain size, β is equal to 10^{-3} mm ($b=10^{-3}$ mm). When the thickness of a weathering rind is measured, the resolution is approximately ±1 mm; therefore, c=1 mm. Measurement of regolith thickness in soil profiles is accomplished at the resolution of about ±1 cm (d=10 mm). Watershed surface area is measured at the resolution of approximately 1 km ($e=10^6$ mm). For each of these measurements, the value of β reflects the minimum asperity on the surface that can be measured. It is important to note that the use of surface area as a scaling factor is based upon an implicit assumption that the weathering rate is interface-limited at all scales; however, weathering rates may be either transport- or interface-limited depending on flow rates in laboratory experiments or hydrological and climate conditions in field studies (Schnoor, 1990; Kump et al., 2000).

Values of Φ_{basalt} can be estimated based on observations of the advance of the weathering front or on solute compositions, as explained in Section 3. If the compositions of the parent and regolith material are known and the system is operating at steady state, then values of w_D^β based on regolith or solutes should be equal. Such equivalence of weathering advance rates determined based on solute and regolith observations has been shown for granitic weathering systems (Stonestrom et al., 1998).

2.1. Laboratory scale

Basalt dissolution experiments (Table 1) yielding rates at the laboratory scale ranging over 3 orders of magnitude are compiled here for comparison (Gislason and Eugster, 1987; Eick et al., 1996; Gislason and Oelkers, 2003). For example, Gislason and Eugster (1987) dissolved both crystalline and glassy basalt in batch reactors at 25 °C at near-neutral values of pH. In these experiments, sodium (Na) and potassium (K) were preferentially released when compared to silicon (Si). Gislason and Oelkers (2003) report dissolution rates calculated from steady state Si concentrations at near-neutral pH for 7, 30 and 50 °C from mixed-flow reactors. They reported that the aluminum to silicon ratio (Al/Si) of the outlet fluid was lower then that of the basaltic glass for experiments with low dissolved concentrations of Al and Si, but that Al/Si was higher than the basaltic glass at high concentrations of Al and Si. In the batch experiments of Eick et al. (1996) Al concentrations were high enough that the reacting fluid was supersaturated with respect to microcrystalline gibbsite; however, no precipitate was observed using electron microscopy.

2.2. Weathering rind and soil profile studies

Weathering advance rates are compiled at the weathering rind scale for basaltic material from Costa Rica (Sak et al., 2004), Japan (Oguchi and Matsukura, 1999), Rocky Mountains, USA (Colman, 1982) and Cascade Mountains in Washington, USA (Porter, 1975) (Table 1). Basaltic clasts from Costa Rica contain plagioclase and augite with trace olivine, ilmenite and magnetite. These clasts are weathering in uplifted river terraces ranging in age from 35 to 250 ka (Sak et al., 2004). Clasts from Japan are closer to andesite in composition and are found in alluvial fan deposits ranging in age from modern to 130 ka (Oguchi and Matsukura, 1999). Samples of Colman (1982) are from glacial till or outwash deposits of Bull Lake (140 ka) glacial stage in Montana and Idaho. Basalt clasts in the Yakima River draining in the Cascade Mountains are from glacial deposits with an estimated age of 14 ka (Porter, 1975, 1976).

One weathering advance rate (Table 1) at the soil profile scale was determined using data from soil pits dug in the Hawi flow along a climosequence at Kohala Mountain on the island of Hawaii (Chadwick et al., 2003). These flows are dominantly mugearite in composition and range in age from 230 to 120 ka as determined from K–Ar dating. The only site in this paper reported to reach bedrock is site E with an approximate age of 150 ka. Depth to bedrock at this site is ~100 cm. Erosion at site E is reported to be minimal due to the position in a slight concavity in the landscape. No other basalt soil profiles have been reported in the literature that provide both exposure age and depth to bedrock.

Table 1
Compilation of weathering advance rates

Reference	Field area	Reported weathering rate	Weathering advance rate, $mm^3\ mm^{-2}\ ky^{-1}$		T, °C	β, mm
			Cations	Si		
Weathering rinds						
[1] Sak et al., 2004	Costa Rica		0.28*		27.3	1
[2] Oguchi and Matsukura, 1999	Japan		0.02*		11.1	1
[3] Colman and Pierce, 1981	McCall, Idaho		0.012*		5.2	1
[4] Colman and Pierce, 1981	Yellowstone, Montana		0.006*		10.2	1
[5] Porter, 1975	Cascade Mtns, Washington		0.018*		4.0	1
Soil profile						
[6] Chadwick et al., 2003	Hawaii—Soil profile		8*		20.0	10
Watersheds						
[7] Dessert et al., 2001	Deccan Traps	37 ton $km^{-2}\ yr^{-1}$	88.1	31.7	25.0	10^6
[8] Dessert et al., 2003	Hawaii	11.9 ton $km^{-2}\ yr^{-1}$	28.3	59.4	16.0	10^6
[9] Dessert et al., 2003	Java	152 ton $km^{-2}\ yr^{-1}$	362	N/A	24.8	10^6
[10] Dessert et al., 2003	Columbia Plateau	7.7 ton $km^{-2}\ yr^{-1}$	18.3	43.6	7.4	10^6
[11] Das et al., 2005	Deccan Traps	11.5 ton $km^{-2}\ yr^{-1}$	27.5	11.8	25.0	10^6
[12] Louvat and Allegre, 1997	Reunion Island	76.5 ton $km^{-2}\ yr^{-1}$	182	75.3	15.0	10^6
[13] Louvat and Allegre, 1998	Sao Miguel	13.3 ton $km^{-2}\ yr^{-1}$	31.6	45.6	16.0	10^6
[14] Gislason et al., 1996	Southwest Iceland	27.2 ton $km^{-2}\ yr^{-1}$	64.8	72.1	5.0	10^6
[15] Gaillardet et al., 2003	Stikine Terrane, Canada	4.1 ton $km^{-2}\ yr^{-1}$	10.8	N/A	2.5	10^6
Laboratory						
[16] Eick et al., 1996	Batch	7.00×10^{-11} mol $m^{-2}\ yr^{-1}$	N/A	6.6×10^{-3}	25	10^{-7}
[17] Gislason and Eugster, 1987	Batch	3.64×10^{-12} mol $m^{-2}\ yr^{-1}$	N/A	3.4×10^{-4}	7	10^{-7}
[18] Gislason and Eugster, 1987	Batch	4.4710^{-12} mol $m^{-2}\ yr^{-2}$	N/A	4.2×10^{-4}	7	10^{-7}
[19] Gislason and Oelkers, 2003	Mixed-flow Reactor	3.97×10^{-11} mol $m^{-2}\ yr^{-3}$	N/A	3.8×10^{-3}	29	10^{-7}
[20] Gislason and Oelkers, 2003	Mixed-flow Reactor	7.39×10^{-11} mol $m^{-2}\ yr^{-4}$	N/A	7.0×10^{-3}	30	10^{-7}
[21] Gislason and Oelkers, 2003	Mixed-flow Reactor	2.1×10^{-10} mol $m^{-2}\ yr^{-5}$	N/A	2.0×10^{-2}	50	10^{-7}
[22] Gislason and Oelkers, 2003	Mixed-flow Reactor	1.78×10^{-11} mol $m^{-2}\ yr^{-6}$	N/A	1.7×10^{-3}	24	10^{-7}
[23] Gislason and Oelkers, 2003	Mixed-flow Reactor	2.61×10^{-10} mol $m^{-2}\ yr^{-7}$	N/A	2.5×10^{-2}	25	10^{-7}

*Calculated directly from measured thickness of soil or weathering rinds.

2.3. Watershed studies

In the literature, watershed denudation rates are reported as either cation denudation rates (Drever, 1994) calculated from release of Na, calcium (Ca), magnesium (Mg) and K, or total denudation rates, calculated from release of Na, Ca, Mg, K and Si (Table 1). For example, two cation denudation rates are reported for the Deccan Traps (Dessert et al., 2001; Das et al., 2005). Das et al. (2005) calculated denudation rates in watersheds underlain by basaltic lithologies, the majority of which are of tholeiitic composition. Dessert et al. (2001) calculated cation denudation rates in three watersheds in the northern Deccan Traps, some of which drain lithologies other than basalt. Weathering advance rates for Java, Hawaii and the Columbia Plateau are calculated from reported cation denudation rates (Dessert et al., 2003). Of these, the cation denudation rates at Java are the highest reported for a basalt watershed to date. Cation denudation rates have also been reported for the Stikine, Skeen and Nass rivers in the Stikine Terrane in Canada (Gaillardet et al., 2003). Numerous basaltic intrusions are reported in the Stikine and Skeen; however, the Nass River, which flows from an area dominated by non-basaltic lithologies, is not included in our compilation. The rocks in the Stikine and Skeen watersheds are not in-place basalt flows but are mostly volcaniclastic sedimentary rocks of basaltic origin and have therefore already experienced one weathering cycle. Total denudation rates for basalt have been reported for Reunion and Sao Miguel Islands (Louvat and Allegre, 1997; Louvat and Allegre, 1998) and for southwest Iceland (Gislason et al., 1996). Input to the watersheds from hydrothermal sources has been recognized on both Sao Miguel and Reunion islands and the authors corrected stream water concentrations to remove hydrothermal contributions.

3. Calculation of weathering advance rates

3.1. Advance rates from water chemistry

Values of Φ_{basalt} at watershed and laboratory scales are calculated from the solute chemistry of streams and outlet solutions, respectively. For example, the value of w^e_{ws} (mm^3 mm^{-2} yr^{-1}) for basalt is calculated from the cation denudation rate normalized to the geographic surface area of the watershed (s^e_{ws}):

$$w^e_{ws} = \left(\frac{q\Sigma m_i}{s^e_{ws}}\right)\left(\frac{1}{\alpha\rho_p(1-\phi)}\right) \quad (2)$$

where m_i is the dissolved concentration (mg mm^{-3}) of element i (i=Na$^+$, Ca^{2+}, Mg^{2+}, K$^+$) and q (mm^3 yr^{-1}) is the average river discharge draining the watershed. Eq. (2) includes the mass of alkali and alkaline earth cations per 100 g parent basalt (α), the porosity of the parent material (ϕ) and the average bulk density of the parent basalt ($\rho_p \cong 2.8$ mg mm^{-3}).

Laboratory dissolution rates were also determined from solute chemistry for batch or mixed-flow reactors. For experiments performed in mixed-flow reactors weathering advance rates are calculated using

$$w^a_{\text{lab}} = \frac{m_{\text{Si}}q}{s^a_{\text{lab}}}\frac{1}{\alpha\rho_p(1-\phi)} \quad (3)$$

where m_{Si} is the Si concentration in the outlet fluids (mg mm^{-3}), q is the fluid flow rate (mm^3 yr^{-1}) and s^a_{lab} is the total BET surface area of the basalt powder in the reactor (mm^2). Weathering advance rates are calculated from batch experiments using

$$w^a_{\text{lab}} = \frac{\mathrm{d}m_{\text{Si}}}{\mathrm{d}t}\frac{1}{s^a_{\text{lab}}}\frac{1}{\alpha\rho_p(1-\phi)} \quad (4)$$

where $\mathrm{d}m_{\text{Si}}/\mathrm{d}t$ is the rate of change in aqueous concentration of Si with time (mg Si mm^{-3} yr^{-1}).

In some cases, researchers report laboratory dissolution rates normalized by geometric surface area. Such a value (w^b_{lab}) can be re-normalized to BET surface area (w^a_{lab}) by multiplying by the so-called roughness value, λ^a_b, the ratio of specific BET surface area (A^b_D, mm^2 mg^{-1}) to specific geometric surface area (A^b_D, mm^2 mg^{-1}) (Helgeson et al., 1984):

$$w^b_{\text{lab}} = w^a_{\text{lab}}\lambda^a_b,\ \lambda^a_b = \frac{A^a_D}{A^b_D}. \quad (5a, b)$$

As we have defined it here, w^β_{ws} (advance rate at the watershed scale) represents the rate at which basalt is transformed into regolith depleted in cations; however the weathering advance rates at the laboratory scale, w^β_{lab}, represent the rate of total dissolution of the basalt based upon Si released to solution. If watershed studies regularly reported total denudation rates where both cations and Si are included in the calculation, w^β_{ws} could be calculated from Si release and compared to w^β_{lab}, however this watershed data is not widely available. For watersheds where total denudation rates were reported, average reported Si concentrations of the study area were used to correct total denudation rates to cation denudation rates before calculation of weathering advance rates using Eq. (2). The difference between calculating w^e_{ws} using concentrations of Si plus cations in stream waters and calculating using cations is less than a factor of 2, a small correction relative to the overall differences recognized across scales (see later discussions). The difference between cation and total denudation rate for a watershed is dependent upon which reactions sequester Si. For example, Si- or Al-containing secondary minerals (gibbsite, kaolinite, halloysite, allophane and amorphous oxides) have been reported in Hawaii, Iceland, and Java (Gislason et al., 1996; Chadwick et al., 2003; Fauzi and Stoops, 2004). Furthermore, biomass takes up and stores Si in phytoliths in leaves in many watersheds (Meunier et al., 1999; Derry et al., 2005).

3.2. Advance rates calculated from regolith thickness

We found no published reports of soil or clast porewater chemistries for basalts that allow estimation of advance rates at the scale of soil profiles and weathering rinds from solute fluxes. Therefore, w^d_{soil} and w^c_{rind} are calculated from observation of advance of the parent-regolith interface as a function of time: the advance rates are equal to the volume of parent material weathered (V_p, mm^3) per total surface area measured at resolution β (s^β_D, mm^2) divided by the duration of time the regolith was exposed to weathering (t, years):

$$w^\beta_D = \frac{V_p}{s^\beta_D}\frac{1}{t}. \quad (6)$$

For isovolumetric weathering without erosion or deposition, $\frac{V_p}{S^\beta_D}$ is simply the regolith thickness divided by the exposure age. However, compaction or expansion can cause the volume of weathered material to differ from the original volume of parent in Eq. (6). This effect is corrected by using the concentration of an immobile element (Brimhall and Dietrich, 1987). Eq. (6) can be rewritten as Eq. (7), where V_p is the original volume of

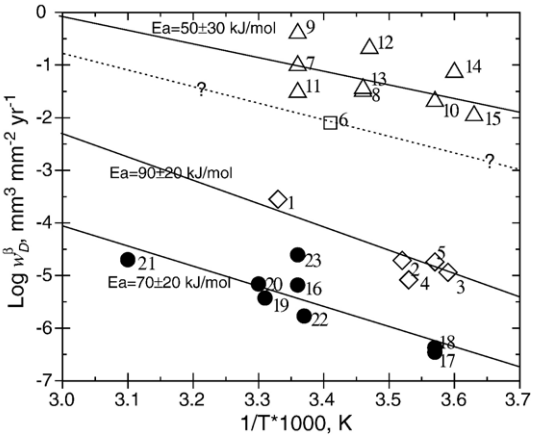

Fig. 2. Arrhenius plot of basalt weathering advance rates calculated at multiple spatial scales ranging from watershed to BET-surface area-normalized laboratory dissolution rates. Open triangles show watershed denudation rates, open squares show soil profile advance rates, open diamonds show weathering rind advance rates, closed circles show BET surface area-normalized laboratory dissolution rates. Average activation energy of basalt weathering calculated across all scales is 70±20 kJ/mol. Solid lines represent the linear fit of data at each scale used to calculate E_a at that scale and the dashed line through the soil profile scale is an estimate of where other soil profile data might plot on this graph (only one such data point was found in the literature). Numbers for each point refer to data in Table 1.

the parent material and $c_{i,p}$ and $c_{i,w}$ equal the concentration of an immobile element such as Ti in the parent and weathered material respectively:

$$w_D^\beta = \frac{V_p \rho_p c_{i,p}}{\rho_w c_{i,w} s_D^\beta} \frac{1}{t}. \quad (7)$$

IF erosion has removed regolith, then the observed weathering advance rate is greater than the true advance rate. For clasts and the soil discussed in this study, physical erosion is absent or minimal (Colman, 1982; Sak et al., 2004; Chadwick et al., 2003). Furthermore, Sak et al. (2004) have shown that the basalt clasts in Costa Rica summarized here weathered iso-volumetrically ($\rho_w c_{i,w} = \rho_p c_{i,p}$). In contrast, soil profiles in Hawaii are inflated by ~10% ($1.1 * \rho_p c_{i,p} = \rho_w c_{i,w}$) due to dust input assuming that the only sourced of the immobile element is from the parent material (Kurtz et al., 2001); therefore, the Hawaiian weathering advance rate calculated directly from regolith thickness may underpredict advance rates by up to 10%.

4. Results and discussion

Weathering advance rates measured at a given mean annual temperature calculated at a given scale vary by less than two orders of magnitude (Fig. 2). Rates increase with mean annual temperature and can be fitted to an Arrhenius equation. Apparent activation energies calculated at each scale, E_a, are within a factor of 2. In contrast, weathering advance rates vary across scales over 7 orders of magnitude, with $w^e_{ws} > w^d_{\text{soil}} > w^c_{\text{rind}} > w^a_{\text{lab}}$.

If we adjust all of the weathering advance rates to 25 °C with Eq. (8)

$$\ln\, w_D^{\beta,298} = \ln\, w_D^\beta + \left(\frac{E_a}{R}\left(\frac{1}{T} - \frac{1}{298}\right)\right) \quad (8)$$

where E_a is the activation energy averaged over the whole dataset (E_a=70 kj mol^{-1}) and T is the average annual temperature (Table 1), we can plot weathering advance rates vs. β, the characteristic resolution of the surface area measurement (Fig. 3). We then see that rates increase with β according to:

$$w_D^\beta = 10^{-3.4} \beta^{0.33}. \quad (9)$$

As mentioned in the Introduction, solute transport out of a watershed or a laboratory reactor (Φ_{basalt}, mm^3 yr^{-1}) should increase with s_D^β if the reaction is interface-limited. In contrast, if transport limits solute release, solute transport would be controlled by equilibrium with basaltic material. We implicitly assume that Φ_{basalt} (Eq. (1)) should approximate a constant for any given temperature and pressure (i.e. effects other then temperature and pressure should contribute relatively small variability). For solute transport limited by equilibrium, Φ_{basalt} should vary with

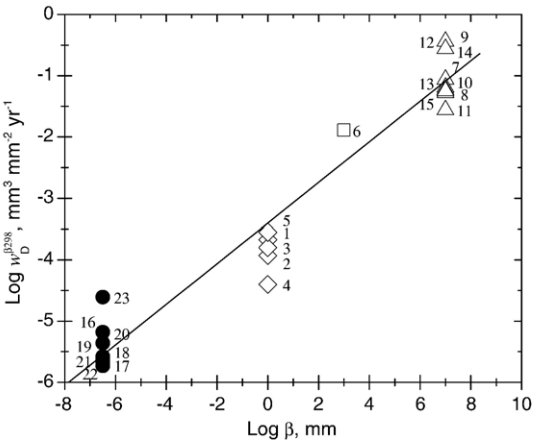

Fig. 3. Weathering advance rate of basalt at 25 °C plotted against the resolution of the surface area measurement at each spatial scale (β). Figure shows that advance rate varies with the scale at which the surface area is measured according to $w_D^\beta = 10^{-3.4}\beta^{0.33}$. Watersheds are plotted as open triangles, soil profile scale as open squares, and weathering rinds as open diamonds. BET surface area-normalized laboratory rates are plotted as closed circles.

temperature according to the van't Hoff equation but should not vary with surface area. For transport-limited systems, then, the value of w_D^β in Eq. (1) would increase with temperature as observed, but decrease with increasing s_D^β. As seen in Fig. 1, however, weathering advance rates in watersheds, clasts, and soils are larger, not smaller, than those estimated in the laboratory. Fig. 3 is consistent with the inference that interface-limitation controls basalt weathering but that the normalization of Φ_{basalt} by s_D^β in Eq. (1) is inappropriate.

According to Mandelbrot (1982), a property such as dissolution rate (Fig. 3), that varies with the scale of measurement can be described with a fractal dimension. The roughness fractal dimension (d_r) is therefore defined and can be determined from the slope (m_r) of a plot of log (weathering advance rate) vs. log β (Mandelbrot, 1982):

$$\begin{aligned} \log\ w_D^\beta &= m_r \log\beta + \log\ w_D^{\beta,0} \\ d_r &= 2 + m_r \end{aligned} \qquad (10a, b)$$

where $\log\ w_D^{\beta,0}$ is equal to the weathering advance rate normalized to surface area measured at a resolution of 1 mm. We assume that variability in weathering advance rate is related to the scale at which surface area is measured and use Eq. (10) to calculate the roughness fractal dimension, d_r, of basalt surface area. In the case of a Euclidean plane, surface area measured at all scales is the same; therefore, m_r equals 0 and d_r equals 2, the fractal dimension for Euclidean geometries. For natural surfaces, as β increases, the size of the minimum surface asperity that is measurable also increases. The roughness fractal dimension of basalt surface area (d_r) ≈ 2.3 (Fig. 3).

If variation in w_D^β across scales arises only because we have used rulers with different resolution to measure surface area, then a weathering advance rate calculated using surface area measured with the same scale ruler should be equal at any scale. In the next section we seek to calculate weathering advance rates at each scale normalized to BET surface area.

4.1. BET surface area-normalized rates

If the BET surface area at any scale is known we can calculate the BET-normalized weathering advance rate (w_D^a):

$$w_D^a = \frac{\Phi_{\text{basalt}}}{s_D^a}. \qquad (11)$$

Although the values of s_D^a have been estimated for some non-basaltic field systems, this parameter has not been estimated for watersheds, soils and rinds developed on basaltic rocks. For non-basaltic systems, values of this parameter have been generally calculated assuming an average specific surface area (BET) of particles (A_D^a, $\text{mm}^2\ \text{mg}^{-1}$) dissolving across a reaction front of average thickness, h (Fig. 1) (Murphy et al., 1998):

$$s_D^a = s_D^\beta h(1-\phi)\rho_p A_D^a. \qquad (12)$$

By substituting Eq. (12) into (11), weathering advance rates from watersheds, soils and rinds can be converted to BET surface area-normalized dissolution rates (w_D^a):

$$w_D^a = \frac{w_D^\beta}{hA_D^a\rho_p(1-\phi)}. \qquad (13)$$

Eq. (13) is used to calculate w_D^a at each value of D using $h=1$ mm as observed in weathering rinds from Costa Rica and $h=500$ mm as observed for the soil at site E in Hawaii (Chadwick et al., 2003). A minimum value of $h=1$ m was estimated for watersheds where large-scale fracturing and development of corestones are assumed to define a thicker reaction front (no appropriate field observations are reported for any of the compiled studies). For watershed, soil, and rind studies, average values of A_D^a are unknown; therefore, the average A_{lab}^a for basalt reported from laboratory experiments compiled in Table 1 ($93\ \text{mm}^2\ \text{mg}^{-1}$) has been used in Eq. (13).

When rates at all scales are normalized to this BET specific surface area, we find that $w_{\text{lab}}^a > w_{\text{rind}}^a, w_{\text{soil}}^a, w_{ws}^a$ (Fig. 4). This is opposite the trend seen in Fig. 3 but is consistent with the so-called laboratory-field discrepancy observed for many systems and minerals where laboratory-measured reaction rates are generally 2–5 orders of magnitude faster then field-measured rates (White et al., 2001; White and Brantley, 2003). Furthermore, if our value of h is underestimated as might be expected given the thick nature of regolith in many altering basaltic regimes, the field rates in Fig. 4 are maximum values of w_{ws}^a. Apparently, our assumption of A_D^a equal to A_{lab}^a at all scales cannot predict BET-normalized rates across scales.

Assuming that w_{lab}^a is equal to w_D^a, in a system like the Hawaiian soil, where the reaction front thickness is known, A_D^a can be determined from Eq. (22) by substituting in values for h (500 mm), ρ_p ($2.8\ \text{mg mm}^{-3}$), ϕ (5%), w_{lab}^a (6.9×10^{-3} mm yr^{-1}), and the measured advance rate for Hawaii (8×10^{-3} mm yr^{-1}). For the Hawaiian soil we calculate a value of $8.7\ \text{mm}^2\ \text{mg}^{-1}$ for A_D^a. This value is an order of magnitude lower than that reported for laboratory dissolution rates and suggests that the average grain size in a reaction front in the field is larger than that used in laboratory experiments.

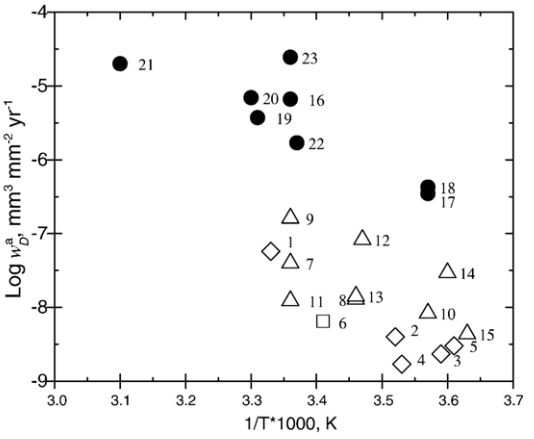

Fig. 4. BET surface area-normalized weathering advance rates estimated using Eq. (13) for laboratory experiments (closed circles), watersheds (open triangles), weathering rinds (open diamonds) and soil (open square). When weathering advance rates are normalized to BET surface area, the familiar laboratory (closed symbols)-field (open symbols) rate discrepancy of 2–5 orders of magnitude can be seen.

4.2. BET surface area-normalized rates from fractal dimensions

We seek another approach to calculate an appropriate surface area for scaling. As previously introduced in Eqs. (5a) and (5b), the roughness has generally been used by geochemists to describe the ratio of the BET to the geometric surface area for a mineral powder (Brantley et al., 1999; Brantley and Mellott, 2000). Roughness can be extended using Eqs. (5b), (9), and (10 to compare weathering advance rates at varying spatial scales to BET surface area-normalized rates:

$$\lambda_\beta^a = \frac{w_D^\beta}{w_D^a} = \frac{A_D^a}{A_D^\beta} = \left(\frac{\beta}{a}\right)^{d_r-2} = \left(\frac{\beta}{a}\right)^{0.33}. \quad (14)$$

Here we have inserted the value of d_r observed from Fig. 3. Assuming that $a=10^{-7}$ mm (Table 2), Eq. (14) can be used to calculate roughness relative to BET scale using d_r:

$$\lambda_\beta^a \approx 200\beta^{0.33}. \quad (15)$$

Roughness therefore increases with β (Table 2): for the watershed ($\beta=e$) roughness = ~20,000 while for geometric ($\beta=b$) roughness = ~20. This latter value is consistent with observed values (e.g. White and Peterson, 1990; White and Brantley, 2003).

By using Eq. (14) or (15), w_D^β (an advance rate from a watershed ($\beta=e$), a saprolite-parent interface advance rate (β=d), or a rind advance rate on a clast ($\beta=c$)) can be re-normalized to a BET surface area using $d_r=2.3$, $a=10^{-7}$ mm, and the appropriate value of β:

$$w_D^\beta = w_D^a \lambda_\beta^a = 200\beta^{0.33} w_D^a. \quad (16)$$

When plotted on an Arrhenius diagram, these scaled values of w_D^a show about two orders of magnitude variation at any given temperature (Fig. 5). Therefore, by using the fractal dimension and the concept of roughness to rescale the weathering advance rates we have reduced the variability exhibited in Fig. 3 significantly. Eq. (16) allows comparison of weathering advance rates scaled to the same resolution of surface area measurement (i.e. BET, $\beta=a$).

Table 2
Scaling values at 25 °C

D	β, mm	$w_D^{\beta,298}$, mm ky^{-1} Eq. (17)	λ_a^β Eq. (15)
lab-BET	$a=1\times10^{-7}$	6.9×10^{-3}	1
lab-geo	$b=1\times10^{-3}$	0.2	20
ws	$c=1$	1.5	200
soil	$d=10$	3.0	430
ws	$e=1\times10^{6}$	140.0	20,000

d_r=2.3.
d_s=2.7.

4.3. Predicting weathering advance rates across scales

The approach outlined here also allows prediction of average weathering advance rates for basalt in the field

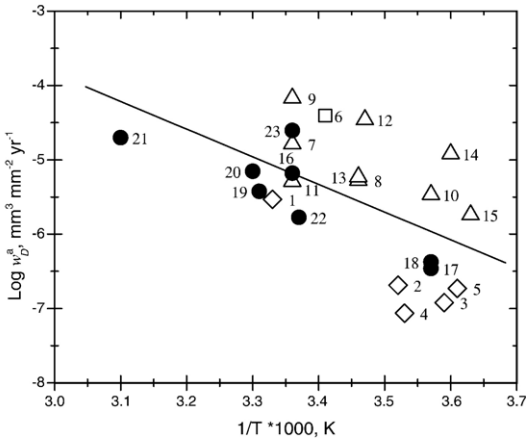

Fig. 5. Values of weathering advance rates scaled to BET surface area at every scale D (w_D^a) calculated using Eq. (17) plotted vs. 1/T. The average activation energy of basalt weathering used in Eq. (17) (70±20 kj mol^{-1}) is equal to the average activation energy calculated across scales from Fig. 2. Laboratory experiments are shown as closed circles for rates normalized by BET surface area and as closed triangles for rates normalized by geometric surface area. Field data are shown as open diamonds, squares, and triangles for weathering rind, soil profile and watershed-scale values, respectively.

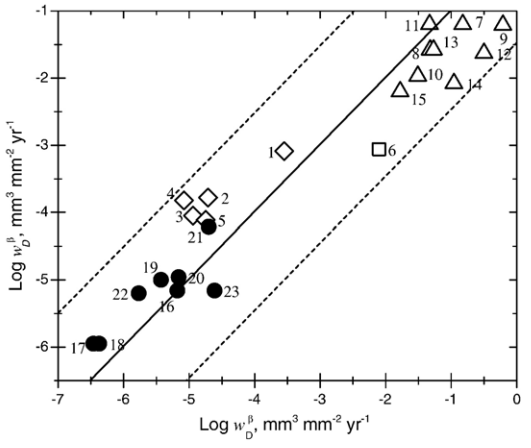

Fig. 6. Values of weathering advance rates calculated from Eq. (17) (w_D^β) compared to w_D^β gleaned from published observations (Table 1). The R^2 value for the linear fit with slope of 1 (solid line) is 0.85 and all but one point lies within the 95% confidence intervals (dashed lines). Laboratory experiments are shown as closed circles for rates normalized by BET surface area. Field data are shown as open diamonds, squares, and triangles for weathering rind, soil profile and watershed-scale values, respectively.

or laboratory using the customary ruler of surface area measurement at that scale and the average activation energy. Using the fractal dimension, d_r, and Eq. (14), the weathering advance rate at any scale (w_D^β) and temperature can be predicted from the weathering advance rate at BET scale (d_r=2.33):

$$w_D^\beta = k_0 \left(\frac{\beta}{a}\right)^{d_r-2} e^{-E_a/RT}. \quad (17)$$

Eq. (17) is a direct consequence of the relationship observed in Fig. 3 as described by Eq. (9). Here, E_a is the average activation energy across all scales (70 kj mol^{-1}) from Fig. 2 and k_0 is the pre-exponential factor (=1.29×10^7 mm^3 mm^{-2} yr^{-1}). In effect, Eq. (17) describes a best estimate of the weathering rate at every scale based upon all measured weathering rates in Table 1 (Fig. 6, Table 2). Interestingly, among the predicted rates, the laboratory rates no longer are the fastest rates among the compilation.

Our approach (and specifically Eq. (17)) can be used to estimate watershed-scale fluxes based on all measured weathering advance rates at all scales. The total CO_2 consumed each year by the weathering of basalt (f_{CO_2}, mol yr^{-1}) at an average temperature of 14 °C (Dessert et al., 2003) can be calculated from Eq. (18),

$$f_{CO_2} = k_0 e^{\frac{-E_a}{RT}} \left(\frac{e}{a}\right)^{d_r-2} \frac{s^e_{\text{globe}} \rho_{\text{basalt}} (1-\phi) \varepsilon_{CO_2}}{M_{\text{basalt}}} \quad (18)$$

where s^e_{globe} is equal to the Earth's total geographic surface area of basalt (7.25×10^6 km^2, Dessert et al., 2003). Here, M_{basalt} (the molecular weight of basalt, 125 g mol^{-1} estimated from the basalt formula in Eq. (19)) and ε_{CO_2} (2.5 mol of CO_2 consumed per mole of basalt weathered) are consistent with the following general basalt weathering reaction:

$$Ca_{0.3}Mg_{0.1}Fe_{0.4}Al_{0.3}SiO_{3.25} + 2.5CO_2 + 3.25H_2O \rightarrow 0.3Ca^{2+} + 0.1Mg^{2+} + 0.4Fe^{2+} + 0.3Al^{3+} + H_4SiO_4 + 2.5HCO_3^- . \quad (19)$$

The total global CO_2 consumed by basalt weathering annually, calculated using Eq. (18) (based on rates at all scales), is 1.75×10^{13} mol CO_2. This estimate is 4.3 times that of the previous estimate of 4.08×10^{12} mol CO_2 yr^{-1} from Dessert et al. (2003) based on bicarbonate concentrations of large rivers and is within the variability that we expect based upon Fig. 6.

It is clear from Figs. 5 and 6 that while surface area discrepancies account for variation in w_D^β of ~4 orders of magnitude across scales, they do not explain the entire scatter in the data. The residuals documented in Fig. 6 must be explained by factors such as differences in dissolution mechanism and rate-limiting step, erosional regime, weathering products, basaltic composition, biotic effects, or climate. For example, varying amounts of smectite (a clay that may contain Ca, Mg, Na and K), kaolinite and gibbsite have been reported in basaltic terrain including the Deccan Traps, southwest Iceland, Java and Reunion (Gislason et al., 1996; Mulyanto and Stoops, 2003; Fauzi and Stoops, 2004; Das et al., 2005) indicating that not all cations that are released to solution stay in solution; therefore, values of w_{ws}^β are minimum estimates. Likewise, fluid in a laboratory dissolution experiment may reach equilibrium with respect to secondary minerals and precipitates may form that lower the concentrations in the outlet fluid and therefore also lower the calculated value of w_{lab}^β. (We note however, that precipitates containing Si were not reported in the compiled studies). Furthermore, w_D^β may vary because secondary minerals formed in the laboratory may differ from those in field settings (Murphy et al., 1998).

Differences in transport vs. interface limitation can also cause variation in both w_D^α and w_D^β. In the case of laboratory studies compiled in this paper, measured dissolution rates are interface-, rather than transport-limited (Gislason and Eugster, 1987; Eick et al., 1996; Gislason and Oelkers, 2003). In contrast, weathering in advection-dominated field systems probably depends upon both transport and kinetics (e.g. West et al., 2005). At low flow rates, dissolution may be limited by transport

while at higher flow rates, dissolution may become interface-limited (Schnoor, 1990). For example, development of weathering rinds on low-porosity clasts wherein transport is dominated by diffusion is transport limited (Berner, 1978, 1981; Kump et al., 2000). Where rates are transport limited rather than interface-limited, as assumed in Eq. (17), predicted weathering rind advance rates will be faster than measured advance rates (Fig. 6).

Physical erosion rates can also influence weathering advance rates (Gaillardet et al., 1999; Riebe et al., 2001, 2003). For the data compiled here, the only systems where physical erosion is occurring are those measured at the watershed scale; therefore, variations in weathering advance rates due to erosion are not expected to be any greater than the variation seen at the watershed scale (e.g. 1–2 orders of magnitude, Fig. 3). For a watershed at steady state, erosion rates equal weathering advance rates and soil/saprolite thickness is constant with time. However, available stream load data for several basalt watersheds (Gislason et al., 1996; Louvat and Allegre, 1997; Louvat and Allegre, 1998; Dessert et al., 2001; Gaillardet et al., 2003) indicate that physical erosion rates are higher than w^e_{ws}, consistent with non-steady state-systems (Stallard, 1992). For the assumption of steady-state soil thickness (Riebe et al., 2004; Fletcher et al., 2006) to be generally true in basalt watersheds undergoing iso-volumetric weathering, either sediment load measurements overestimate long term physical erosion or weathering advance rates in these systems must be increasing over time to achieve balance with physical erosion rates.

5. Fractal dimensions and reaction front geometry

So far, our treatment has not provided a conceptual framework for the scaling parameters. According to Eq. (12) the total BET surface area of a watershed is dependent upon both the reaction front thickness and the specific BET surface area, where specific BET surface area is related to the size of particles in the reaction front. In order to understand the nature of this BET surface area, we investigate how the specific surface area of powdered basalt varies as a function of the grain radius (r).

The slope (m_s) of a plot of log specific BET surface area of laboratory ground basalt grains vs. log r defines the surface fractal dimension, d_s (Farin and Avnir, 1987):

$$\log A^a_D = m_s \log r + \log A^{a,0}_D \qquad d_s = m_s + 3 \qquad (20a, b)$$

where $A^{a,0}_D$ is the BET specific surface area of a 1 mm grain (52 mm^2 mg). If grains are perfect Euclidean spheres, then $m_s = -1$ and $d_s = 2$, the fractal dimension of a planar surface (Mandelbrot, 1982). In reality, grains are not perfect spheres and therefore $d_s > 2$ due to surface roughness. Fractal dimension approaches 3 for space-filling surfaces. A plot of log A^a_{lab} vs. log r (Fig. 7) for laboratory-ground natural basaltic glass powders shows that BET surface area varies with grain size (Papelis et al., 2003) such that $d_s \approx 2.7$ and log $A^{a,0}_{lab} = 4.7$ mm^2 g^{-1}. Similar slopes of log A^a_{lab} vs. log r are reported for plagioclase of varying composition ground in the laboratory (m_s ranging from −0.23 to −0.5), yielding d_s ranging from 2.8 to 2.5 (Brantley et al., 1999 and references within; Holdren and Speyer, 1987). Eq. (20) could be used to calculate total BET surface area of a reaction front with a known grain size distribution. However, grain size distribution is rarely measured. Instead, we assume that there is an average or characteristic grain size at each scale β (r^β_{av}) that can be used to predict the specific BET surface area using Eq. (20). With that assumption, then the roughness value in Eq. (14) can be rewritten in terms of r_{av}:

$$\lambda^a_\beta = \left(\frac{\beta}{a}\right)^{d_r - 2} = \left(\frac{r^a_{av}}{r^\beta_{av}}\right)^{d_s - 3}. \qquad (21)$$

Similar to rescaling weathering advance rates using β in Eq. (17), we can also scale weathering advance rates based on this characteristic grain size (r^β_{av}). Eq. (21) provides a relationship between d_r and d_s that allows rewriting of Eq. (17) as a function of r_{av}:

$$w^\beta_D = k_0 \left(\frac{r^a_{av}}{r^\beta_{av}}\right)^{d_s - 3} e^{-E_a/RT}. \qquad (22)$$

To extrapolate basalt weathering advance rates across scales either requires a value of d_r (Eq. (17)) or d_s

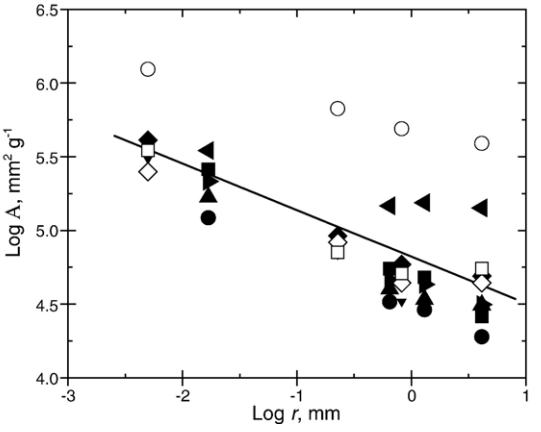

Fig. 7. BET specific surface area measured on laboratory ground natural basalt glasses as a function of grain radius (Papelis et al., 2003). Different symbols represent samples from different geographic locations. Slope of linear fit through all the data is −0.32.

(Eq. (22)). The two fractal dimensions allow extrapolation from either of the two critical scales of measurement of the weathering front: h, reaction front thickness (or the maximum height of an undulation in the front that is measured at scale D), or β, the minimum height of an asperity on the front that is measured with ruler of resolution β. As the scale of measurement increases from laboratory to field, the maximum dimension of an undulation (h) that is incorporated in the system increases.

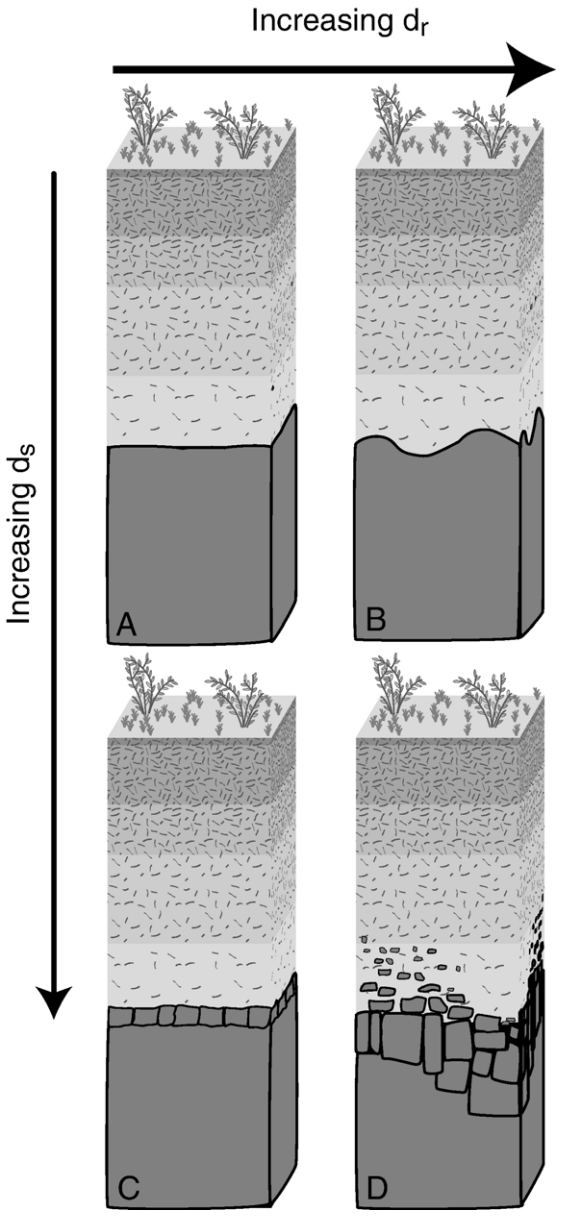

Fig. 8. Schematic diagram indicating how the weathering front roughness varies with both d_s and d_r. For an infinitely thin, absolutely planar reaction front with no fractures or corestones, $d_r=d_s=2$ (A). $d_r>2$ represents undulations in the bedrock saprolite contact (B) while $d_s>2$ represents more particles within the reaction front (C). For natural reaction fronts, d_r and d_s are both greater than 2, representing both an undulating front that is likely not constant thickness and a distribution of particles sizes within the front (D).

A reaction front that is infinitely thin and completely planar (Euclidean) is represented by $d_r=d_s=2$ (Fig. 8A). A reaction front where d_r is greater than 2 but d_s is equal to 2 represents an undulating but planar surface (Fig. 8B). Alternately, we can conceptualize a reaction front where d_r is equal to 2 but d_s is greater than 2 as a plane of particles that make up the reaction front (Fig. 8C). In this case, $r_{av}=h$. In reality, reaction fronts are probably characterized by d_r, $d_s>2$ where $h\neq r_{av}$ as depicted in Fig. 8D.

Manipulation of Eq. (21) also elucidates how to think about the natural weathering interface:

$$\frac{\left(\frac{\beta}{a}\right)^2}{\left(\frac{r_{av}^a}{r_{av}^\beta}\right)^3}=\frac{\left(\frac{\beta}{a}\right)^{d_r}}{\left(\frac{r_{av}^a}{r_{av}^\beta}\right)^{d_s}}. \tag{23}$$

This formulation emphasizes that $d_r\neq d_s$. Indeed, d_r/d_s is expected to equal 2/3, a value which is not too different than the value we have suggested for basalt (0.85). We have shown how to address roughness of the weathering interface with either d_r (Fig. 8B) or d_s (Fig. 8C).

6. Conclusions

The apparent activation energy for all basalt weathering rates assuming a roughness fractal dimension=2.3 is 70 ± 20 kJ mol^{-1}. This value compares well with values of activation energy estimated by Sak et al. (2004), 51 kJ mol^{-1}, for weathering rinds developed on basalt clasts. The value is larger than that estimated by Dessert et al. (2001), 42.3 kJ mol^{-1} as calculated from bicarbonate concentrations in rivers. Activation energies reported for laboratory experiments range from 25.5 kJ mol^{-1} (Gislason and Oelkers, 2003) to 32 ± 3 kJ mol^{-1} (Gislason and Eugster, 1987) for basalt.

The issue of scaling (either up or down) measurements or observations from different spatial or temporal scales has been discussed by many researchers in the context of the laboratory-field discrepancy (e.g. Velbel, 1993; Pope et al., 1995; Viles, 2001; White and Brantley, 2003). We find that the largest source of variation in weathering advance rates across spatial scales is attributed to the inability to measure comparable surface area at different scales. A fractal dimension can therefore be used to calculate appropriate surface areas at each scale to reduce the scaling discrepancy. The remaining

small variations in weathering advance rate within each scale can be attributed to other factors influencing weathering rates such as weathering regime, erosion, biological activity and composition of secondary minerals. Roughness at each scale is partly determined by the measuring resolution at a given scale and partly determined by the weathering mechanism at each scale. Basalt weathering advance rates at any scale can be predicted from BET-normalized weathering advance rates by using the activation energy (70 kj mol^{-1}) and the roughness fractal dimension for basalt weathering ($d_r \approx 2.3$) using Eq. (17). Alternately, the weathering advance rate can be related to the surface fractal dimension and a characteristic grain dimension using Eq. (22).

The approach outlined here should be useful for other weathering lithologies and will provide some insight into the reaction front geometry when combined with fractal analysis of surface area variation with grain size. However, the roughness fractal dimension is not expected to be the same for all lithologies. For example, for granite we hypothesize that the weathering interface is more Euclidean (less space-filling) because fracture density in weathering granites is generally lower than weathering basalts, and the roughness fractal dimension should be closer to 2. Future research will extend this work to other lithologies.

Acknowledgements

This material is based upon work supported by the National Science Foundation under Grant Numbers CHE-0431328 and DGE-9972759. We thank B. Carrey and an anonymous reviewer for constructive reviews of this manuscript.

References

Berner, R.A., 1978. Rate control of mineral dissolution under Earth surface conditions. Am. J. Sci. 278, 1235–1252.

Berner, R.A., 1981. Kinetics of weathering and diagenesis. Rev. Miner. 8, 111–134.

Berner, R.A., Lasaga, A.C., Garrels, R.M., 1983. The carbonate–silicate geochemical cycles and its effect on atmospheric carbon dioxide over the past 100 million years. Am. J. Sci. 283, 641–683.

Brantley, S.L., 2003. Reaction kinetics of primary rock-forming minerals under ambient Conditions, *in* Fresh Water Geochemistry, Weathering, and Soils, J.I. Drever (ed.), v. 5 of Treatise on Geochemistry, K.K. Turekian and H.D. Holland (eds.), Pergamon Press, Oxford, 73–118.

Brantley, S.L., Mellott, N.P., 2000. Surface area and porosity of primary silicate minerals. Am. Mineral. 85, 1767–1783.

Brantley, S.L., White, A.F., Hodson, M.E., 1999. Surface area of primary silicate minerals. In: Jamtveit, B., Meakin, P. (Eds.), Growth, Dissolution and Pattern Formation in Geosystems. Kluwer Academic Publishers, Netherlands, pp. 291–326.

Brimhall, G.H., Dietrich, W.E., 1987. Constitutive mass balance relations between chemical composition, volume, density, porosity, and strain in metasomatic hydrochemical systems: results on weathering and pedogenesis. Geochim. Cosmochim. Acta 51, 567–587.

Brunauer, S., Emmett, P.H., Teller, E., 1938. Adsorption of gases in multimolecular layers. J. Am. Chem. Soc. 60.

Burch, T.E., Nagy, K.L., Lasaga, A.C., 1993. Free-Energy Dependence of Albite Dissolution Kinetics at 80-Degrees-C and Ph 8.8. Chem. Geol. 105, 137–162.

Chadwick, O.A., Gavenda, R.T., Kelly, E.F., Ziegler, K., Olson, C.G., Elliott, W.C., Hendricks, D.M., 2003. The impact of climate on the biogeochemical functioning of volcanic soils. Chem. Geol. 202, 195–223.

Colman, S.M., 1982. Clay mineralogy of weathering rinds and possible implications concerning the sources of clay minerals in soil. Geology 10, 370–375.

Colman, S.M., Pierce, K.L., 1981. Weathering rinds on andesitic and basaltic stones as a Quaternary age indicator, Western United States. U. S. Geol. Surv. Prof. Pap., vol. 1210. Washington, DC.

Das, A., Krishnaswami, S., Sarin, M.M., Pande, K., 2005. Chemical weathering in the Krishna Basin and Western Ghats of the Deccan Traps, India: rates of basalt weathering and their controls. Geochim. Cosmochim. Acta 69, 2067–2084.

Derry, L.A., Kurtz, A.C., Ziegler, K., Chadwick, O.A., 2005. Biological control of terrestrial silica cycling and export fluxes to watersheds. Nature 433, 728–731.

Dessert, C., Dupre, B., Francois, L., Schott, J., Gaillardet, J., Chakrapani, G.J., Bajpai, S., 2001. Erosion of Deccan Traps determined by river geochemistry: impact on the global climate and the $^{87}Sr/^{86}Sr$ ratio of seawater. Earth Planet. Sci. Lett. 188, 459–474.

Dessert, C., Dupre, B., Gaillardet, J., Francois, L., Allegre, C., 2003. Basalt weathering laws and the impact of basalt weathering on the global carbon cycle. Chem. Geol. 202, 257–273.

Drever, J.I., 1994. The effect of land plants on weathering rates of silicate minerals. Geochim. Cosmochim. Acta 58, 2325–2332.

Drever, J.I., Clow, D.W., 1995. Weathering rates in catchments. In: White, A., Brantley, S. (Eds.), Chemical Weathering Rates of Silicate Minerals. Mineralogical Society of America, Washington D.C, pp. 463–483.

Drever, J.I., Stillings, L.L., 1997. The role of organic acids in mineral weathering. Colloids Surf. 120, 167–181.

Eick, M.J., Grossl, P.R., Golden, D.C., Sparks, D.L., Ming, D.W., 1996. Dissolution of a lunar basalt simulant as affected by pH and organic anions. Geoderma 74, 139–160.

Farin, D., Avnir, D., 1987. Reactive fractal surfaces. J. Phys. Chem. 91, 5517–5521.

Fauzi, A.I., Stoops, G., 2004. Reconstruction of a toposequence on volcanic material in the Honje Mountains, Ujung Kulon Peninsula, West Java. Catena 56, 45–66.

Fletcher, R.C., Buss, H.L., Brantley, S.L., 2006. A spheroidal weathering model coupling porewater chemistry to soil thicknesses during steady-state denudation. Earth Planet. Sci. Lett. 244, 444–457.

Gaillardet, J., Dupre, B., Louvat, P., Allegre, C., 1999. Global silicate weathering and CO_2 consumption rates deduced from the chemistry of large rivers. Chem. Geol. 159, 3–30.

Gaillardet, J., Millot, R., Dupre, B., 2003. Chemical denudation rates of the western Canadian orogenic belt: the Stikine terrane. Chem. Geol. 201, 257–279.

Gislason, S., Eugster, H.P., 1987. Meteoric water–basalt interaction. I: a laboratory study. Geochim. Cosmochim. Acta 51, 2827–2840.

Gislason, S., Oelkers, E., 2003. Mechanism, rates and consequences of basaltic glass dissolution: II. an experimental study of the dissoltuion

rates of basaltic glass as a function of pH and temperature. Geochim. Cosmochim. Acta 67, 3817–3832.

Gislason, S., Arnorsson, S., Armannson, H., 1996. Chemical weathering of basalt in southwest Iceland: effects of runoff, age of rocks and vegetative/glacial cover. Am. J. Sci. 296, 837–907.

Helgeson, H.C., Murphy, W.M., Aagard, P., 1984. Thermodynamic and kinetic constraints on reaction rates among minerals and aqueous solutions II. Rate constants, effective surface area, and the hydrolysis of feldspar. Geochim. Cosmochim. Acta 48, 2405–2432.

Hedin, L.O., Vitousek, P.M., Matson, P.A., 2003. Nutrient losses over four million years of tropical forest development. Ecology 84, 2231–2255.

Hodson, M.E., 2006. Searching for the perfect surface area normalizing term—a comparison of BET surface area-, geometric surface area- and mass-normalized dissolution rates of anorthite and biotite. J. Geochem. Explor. 88, 288–291.

Holdren, G.R., Speyer, P.M., 1987. Reaction rate surface area relationships during the early stages of weathering; II. Data on eight additional feldspars. Geochim. Cosmochim. Acta 51, 2311–2318.

Johnson, N., Driscoll, C., Eaton, J., Liken, G., McDowell, W., 1981. 'Acid rain', dissolved aluminum and chemical weathering at the Hubbard Brook Experimental Forest, New Hampshire. Geochim. Cosmochim. Acta 45, 1421–1437.

Kump, L., Brantley, S.L., Arthur, M., 2000. Chemical Weathering, Atmospheric CO_2, and Climate. Annu. Rev. Earth Planet. Sci. 28, 611–667.

Kurtz, A.C., Derry, L.A., Chadwick, O.A., 2001. Accretion of Asian dust to Hawaiian soils: isotopic, elemental, and mineral mass balances. Geochim. Cosmochim. Acta 65, 1971–1983.

Louvat, P., Allegre, C.J., 1997. Present denudation rates on the island of Reunion determined by river geochemistry: basalt weathering and mass budget between chemical and mechanical erosions. Geochim. Cosmochim. Acta 61, 3645–3669.

Louvat, P., Allegre, C.J., 1998. Riverine erosion rates on Sao Miguel volcanic island, Azores archipelago. Chem. Geol. 148, 177–200.

Lucas, Y., 2001. The role of plants in controlling rates and products of weathering: importance of biological pumping. Annu. Rev. Earth Planet. Sci. 29, 135–163.

Mandelbrot, B., 1982. The Fractal Geometry of Nature. Freeman, San Francisco, CA.

Meunier, J.D., Colin, F., Alarcon, C., 1999. Biogenic silica storage in soils. Geology 27, 835–838.

Mulyanto, B., Stoops, G., 2003. Mineral neoformation in pore spaces during alteration and weathering of andesitic rocks in humid tropical Indonesia. Catena 54, 385–391.

Murphy, S.F., Brantley, S.L., Blum, A.E., White, A.F., Dong, H., 1998. Chemical weathering in a tropical watershed, Luquillo Mountain, Puerto Rico: I. rate and mechanism of biotite weathering. Geochim. Cosmochim. Acta 62, 2404.

Oelkers, E., Schott, J., Devidal, J., 1994. The effect of aluminum, pH and chemical affinity on the rates of alumino-silicate dissolution reactions. Geochim. Cosmochim. Acta 58, 2011–2024.

Oguchi, C.T., Matsukura, Y., 1999. Effect of porosity on the increase in weathering-rind thicknesses of andesite gravel. Eng. Geol. 55, 77–89.

Papelis, C., Um, W., Russell, C.E., Chapman, J.B., 2003. Measuring the specific surface area of natual and manmade glasses: effects of formation process, morphology, and particle size. Colloids Surf., A Physicochem. Eng. Asp. 215, 221–239.

Pope, G., Dorn, R., Dixon, J., 1995. A new conceptual model for understanding geographical variations in weathering. Ann. Assoc. Am. Geogr. 85, 38–64.

Porter, S.C., 1975. Weathering rinds as a relative-age criterion—application to subdivision of glacial deposits in cascade-range. Geology 3, 101–104.

Porter, S.C., 1976. Pleistocene Glaciation in Southern Part of North Cascade Range, Washington. Geol. Soc. Amer. Bull. 87, 61–75.

Riebe, C.S., Kirchner, J.W., Granger, D.E., Finkel, R.C., 2001. Strong tectonic and weak climatic control of long-term chemical weathering rates. Geology 29, 511–514.

Riebe, C.S., Kirchner, J.W., Finkel, R.C., 2003. Long-term rates of chemical weathering and physical erosion from cosmogenic nuclides and geochemical mass balance. Geochim. Cosmochim. Acta 67, 4411–4427.

Riebe, C.S., Kirchner, J.W., Finkel, R.C., 2004. Erosional and climatic effects on long-term chemical weathering rates in granitic landscapes spanning diverse climate regimes. Earth Planet. Sci. Lett. 224, 547–562.

Sak, P.B., Fisher, D.M., Gardner, T.W., Murphy, K., Brantley, S.L., 2004. Rates of weathering rind formation on Costa Rican basalt. Geochim. Cosmochim. Acta 68, 1453–1472.

Schnoor, J.L., 1990. Kinetics of chemical weathering: a comparison of laboratory and field weathering rates. In: Stumm, W. (Ed.), Aquatic Chemical Kinetics: Reaction Rates of Processes in Natural Waters. Swiss Federal Institute of Technology, Zurich, pp. 475–504.

Stallard, R., 1992. Tectonic processes, continental freeboard, and the rate-controlling step for continental denudation. In: Butcher, S. (Ed.), Global Biogeochemical Cycles. Academic Press, London.

Stonestrom, D.A., White, A.F.C., Akstin, K., 1998. Determining rates of chemical weathering in soils—solute transport versus profile evolution. J. Hydrol. 209, 331–345.

Swoboda-Colberg, N., Drever, J., 1993. Mineral dissolution rates in plot-scale and laboratory experiments. Chem. Geol. 105, 51–69.

Velbel, M.A., 1993. Constancy of silicate–mineral weathering-rate ratios between natural and experimental weathering: implications for hydrologic control of differences in absolute rates. Chem. Geol. 105, 89–99.

Viles, H., 2001. Scale issues in weathering studies. Geomorphology 41, 63–72.

Walker, J.C.G., Hays, P.B., Kasting, J.F., 1981. A negative feedback mechanism for the long-term stabilization of Earth's surface temperature. J. Geophys. Res. 86, 9776–9782.

West, A.J., Galy, A., Bickle, M., 2005. Tectonic and climatic controls on silicate weathering. Earth Planet. Sci. Lett. 235, 211–228.

White, A.F., 1995. Chemical weathering rates of silicate minerals in soils. In: White, A., Brantley, S. (Eds.), Chemical Weathering Rates of Silicate Minerals. Mineralogical Society of America, Washington D.C., pp. 407–458.

White, A.F., 2002. Determining mineral weathering rates based on solid and solute weathering gradients and velocities: application to biotite weathering in saprolites. Chem. Geol. 190, 69–89.

White, A.F., Brantley, S.L., 1995. Chemical Weathering Rates of Silicate Minerals. Mineralogical Society of America, Washington, D.C.

White, A.F., Brantley, S.L., 2003. The effect of time on the weathering of silicate minerals: why do weathering rates differ in the laboratory and field? Chem. Geol. 202, 479–506.

White, A.F., Peterson, M.L., 1990. Role of reactive surface area characterization in geochemical models, in: D.L. Melchoir, R.L. Bassett, (Eds), Chemical Modeling of Aqueous Systems II 416, American Chemical Society Symposium Series, pp. 461–475.

White, A.F., Bullen, T.D., Schultz, M.S., Blum, J.D., Huntington, T.G., Peters, N.E., 2001. Differential rates of feldspar weathering in granitic regoliths. Geochim. Cosmochim. Acta 65, 847–869.